

Effectiveness and intermediates of microcystin-LR degradation by UV/H₂O₂ via 265 nm ultraviolet light-emitting diodes

Juan Liu, Jin-shao Ye, Hua-se Ou & Jialing Lin

Environmental Science and Pollution Research

ISSN 0944-1344
Volume 24
Number 5

Environ Sci Pollut Res (2017)
24:4676–4684
DOI 10.1007/s11356-016-8148-1



Your article is protected by copyright and all rights are held exclusively by Springer-Verlag Berlin Heidelberg. This e-offprint is for personal use only and shall not be self-archived in electronic repositories. If you wish to self-archive your article, please use the accepted manuscript version for posting on your own website. You may further deposit the accepted manuscript version in any repository, provided it is only made publicly available 12 months after official publication or later and provided acknowledgement is given to the original source of publication and a link is inserted to the published article on Springer's website. The link must be accompanied by the following text: "The final publication is available at link.springer.com".



RESEARCH ARTICLE

Effectiveness and intermediates of microcystin-LR degradation by UV/H₂O₂ via 265 nm ultraviolet light-emitting diodes

Juan Liu¹ · Jin-shao Ye^{1,2} · Hua-se Ou¹ · Jialing Lin¹Received: 11 July 2016 / Accepted: 23 November 2016 / Published online: 14 December 2016
© Springer-Verlag Berlin Heidelberg 2016

Abstract Although the degradation of cyanotoxins by 254 nm UV/H₂O₂ has been well elucidated, the efficiency and mechanism involved are not necessarily true for other UV wavelengths. The degradation of microcystin-LR (MC-LR), a representative cyanotoxin, was explored by UV/H₂O₂ using 265 nm ultraviolet light-emitting diode (UV-LED). The results indicated that 265 nm UV/H₂O₂ treatment had a high removal efficiency of MC-LR ([MC-LR] = 0.1 μM, apparent rate constants reached 0.2077 min⁻¹, half-time at 3.3 min). The qualitative analyses demonstrated that three novel intermediates, C₄₈H₇₄N₁₀O₁₅ (molecular weight = 1030.5335), C₃₆H₅₈N₁₀O₁₄ (854.4134), and C₃₃H₅₄N₁₀O₁₄ (814.3821), were generated in 265 nm UV/H₂O₂. Five published intermediates were also confirmed. The generative pathway of these products mainly involved free hydroxyl radical oxidation, resulting in consecutive hydroxyl substitutions and hydroxyl additions of unsaturated bonds in MC-LR. The toxicity of MC-LR was weakened with a relative low mineralization. The electrical energy per order values were calculated to be in the range of 0.00447 to 0.00612 kWh m⁻³ order⁻¹ for 100–

5000 μg L⁻¹ MC-LR. Overall, 265 nm UV-LED/H₂O₂ can be used as an alternative effective technology to improve the removal efficiency of MC-LR in water.

Keywords Photocatalysis · Cyanotoxin · Hydroxyl radical · Drinking water treatment · Organic matter · Toxicology

Introduction

The frequent episodes of algae/cyanobacterial blooms and the occurrence of cyanotoxins have been extensively reported (Ibelings et al. 2014), and thus, worldwide environmental protection agencies have assigned a high priority to cyanotoxin control (Christoffersen and Kaas 2000; USEPA 2007). Unfortunately, traditional drinking water treatment procedures are believed to have low cyanotoxin removal efficiency. Thus, attempts aimed at seeking efficient methods for cyanotoxin degradation are continuously conducted. A myriad of advanced technologies, such as ozonation (Chang et al. 2014), Fenton oxidation (de Freitas et al. 2013), and chlorine dioxide oxidation (Zhou et al. 2014), have been tested against cyanotoxins, and their efficiencies have been verified. However, their shortcomings cannot be ignored, including complicated operation, dangerous chemical addition, and costly consumable. In contrast, the ultraviolet (UV) technique is very attractive because of its simple operation and high efficacy against pathogens and organic matters. More importantly, UV processes are free of harmful chemical addition and generate fewer by-products. Therefore, UV-based techniques may be more feasible for cyanotoxin removal in drinking water.

UV-inducing degradation of organic matters mainly involves two mechanisms: direct UV photolysis and hydroxyl radical (OH·) advanced oxidation (Vilhunen and Sillanpää

Responsible editor: Vitor Manuel Oliveira Vasconcelos

Electronic supplementary material The online version of this article (doi:10.1007/s11356-016-8148-1) contains supplementary material, which is available to authorized users.

✉ Hua-se Ou
touhuase@jnu.edu.cn

¹ School of Environment, Guangzhou Key Laboratory of Environmental Exposure and Health, and Guangdong Key Laboratory of Environmental Pollution and Health, Jinan University, Guangzhou 510632, China

² Lawrence Berkeley National Laboratory, Joint Genome Institute, Walnut Creek, CA 94598, USA

2010). Most of the published studies regarding cyanotoxins have focused on microcystins, especially microcystin-LR (MC-LR). MC-LR is composed of seven amino acids, which are somewhat susceptible to direct UV irradiation (Fig. S1). UV-C (254 nm) irradiation reportedly induced the isomerization but not degradation of MC-LR in a neutral water body (Kaya and Sano 1998; Tsuji et al. 1995). For UV-B and UV-A, no direct photolysis was reported. In contrast, UV/H₂O₂ and UV/TiO₂ processes can generate highly oxidative OH·, which degraded MC-LR into multiple intermediate products (Fotiou et al. 2013; Zong et al. 2013). The degradation pathways involved the OH· oxidation of several susceptible sites, including the unsaturated double bonds (C=C), the methoxy group, and the benzene ring of Adda, as well as the C=C of Mdha in MC-LR (Antoniou et al. 2008b).

The existing literature regarding MC-LR degradation usually used 254 nm UV wavelength (mercury arc lamp) (Zong et al. 2013) or consecutive emitting wavelengths (xenon lamp) (Liu et al. 2009). Furthermore, the most common UV light source is the mercury arc lamp, which has several weaknesses, such as high energy consumption, toxic heavy metals, frequent lamp replacement, and fragility (Vilhunen and Sillanpää 2010). Thus, the employment of more sustainable UV light sources is urgently needed. Within the last decade, the development of solid-state-producing techniques provided us the compact, low-cost, low-energy, and environmentally friendly light-emitting diodes (LEDs). LED is free of toxicants and emits light at independent narrowband (half bandwidth <10 nm) (Jo and Tayade 2014). Ultraviolet LED (UV-LED), which can emit 200–400 nm UV light, has been developed based on aluminum gallium nitride material (Vilhunen and Sillanpää 2009). Thus, the degrading potential of organic matters using UV-LED would be highly significant. Recently, multifarious reactors based on different wavelength UV-LEDs were developed to degrade indicative organic compounds, including phenol (Jamali et al. 2013), formaldehyde (Chiou et al. 2008), methylene blue (Tayade et al. 2009), methyl red (Repo et al. 2013), and even fulvic acids (Izadifard et al. 2013). These studies preliminarily verified the feasibility of UV-LED, but its ability to degrade complex biological contaminants, such as cyanotoxins, is still unknown.

In the present study, our research group designed a UV-LED micro-module for the degradation experiment. MC-LR was used as an indicative cyanotoxin, and the degrading effectiveness of it using UV-LED/H₂O₂ was evaluated. Moreover, the reaction intermediates and their generative mechanisms were elucidated using a high-resolution tandem mass spectrometry. The cost evaluation was also conducted. The results reported here can be used to develop UV-LED-based techniques for drinking water treatment system.

Materials and methods

Materials and reagents

All chemical reagents in the study were of the highest purity available (Text S1).

UV-LED micro-module

A UV-LED irradiation micro-module was designed and assembled (Fig. 1). This module consisted of five components, including UV-LED array, power source, heat dissipation device, module framework, and reactor vessel. The UV-LED array was composed of nine UV-LED chips (HONGLI Tronic Inc., China), which had the same maximum emitting peak at 265 nm and a half-wave bandwidth of 10 nm. The irradiating intensity was measured using a HAAS-3000 light spectrum irradiation meter (Everfine, China), and the average irradiating intensity of this UV-LED array was approximately 180 μW cm⁻² on the surface of the reaction solution. The irradiation dose was calculated as

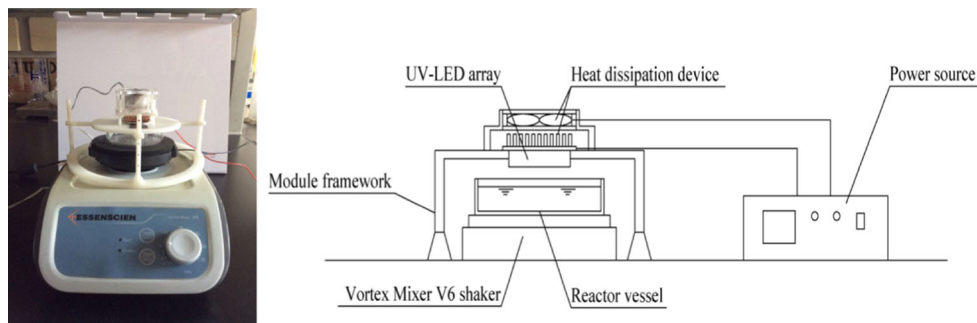
$$\text{Dose} = \text{Int} \times T \quad (1)$$

where Int is the irradiation intensity, *T* is the irradiation time (s), and irradiation dose has a unit of millijoules per square centimeter. The module framework was designed by AutoCAD (Autodesk, USA) and was produced using the laser rapid prototyping technique. A customized circular quartz vessel (6 cm diameter) was used as the reactor vessel.

UV-LED irradiation experiments

Twenty milliliters of MC-LR solution at different initial concentrations (100–5000 μg L⁻¹, 0.1–5.0 μM) was spiked into the quartz vessel. In the UV/H₂O₂ experiments, the initial concentration of H₂O₂ was 3.4 mg L⁻¹ (100 μM). The pH value was maintained in the range of 6.8–7.2 using a 5.0 mM phosphate-buffered solution. The solution was maintained at 25 ± 2 °C, and the uniformity was achieved by shaking the dish at 60 rpm. The reaction was initiated by turning on the UV-LED array. At a pre-defined time, Na₂SO₃ at a concentration stoichiometrically equivalent to the initial H₂O₂ dose was added to stop the reaction. Afterwards, 5 mL of the sample was transferred into a brown amber tube and then stored at 4 °C before sample analysis. UV/H₂O₂-free, UV only, and H₂O₂ only control experiments were included in the experimental design.

Fig. 1 Micro-UV-LED module and its schematic diagram



HPLC separation

The samples were injected into a LC-20A liquid chromatography system (Shimadzu, Japan) with a Shim-pack XR-ODS column (2.0×100 mm, $2.2 \mu\text{m}$, 120 \AA) prior to the MS analysis. The injection volume was $10 \mu\text{L}$, and the mobile phase was a gradient elution of water (mobile phase A) and acetonitrile (mobile phase B), both containing 0.1% formic acid. The gradient elution was programmed as follows: 0–8.0 min, 5–90% B; 8.0–10.0 min, 90% B; 10.0–10.1 min, 90–5% B; and 10.1–15.0 min, 5% B ($30 \text{ }^\circ\text{C}$, 0.2 mL min^{-1}).

Reaction intermediate analysis

The identification of intermediates was performed using a TripleTOF 5600+ high-resolution tandem mass spectrometry (HRMS) (Applied Biosystems SCIEX, USA). The instrumentation conditions are listed in Table S1. Nitrogen served both as the turbo and the collision gas. Mass calibrations and resolution adjustments on the quadrupoles and TOF were performed automatically using a 10^{-5} M solution of polypropylene glycol introduced via a model II Harvard infusion pump. The scan range was set at m/z 100–1200. The data were analyzed using PeakView and MasterView (Applied Biosystems SCIEX, USA). A systematic intermediate screening procedure was conducted (Text S2).

Quantitative analysis of MC-LR and its intermediates

The quantitative analysis of MC-LR and intermediates was performed using a TripleQuad 5500 tandem mass spectrometry (Applied Biosystems SCIEX, USA). Most of the instrumentation conditions were similar to those of 5600+ system, but the collision-induced dissociation (CID) energy was optimized for different intermediates. The scan mode was multireaction monitoring, and the monitoring ion pairs are listed in Table S2.

Total organic carbon analysis and computational methods of MC-LR properties

The TOC value was measured using a LiquiTOC trace analyzer (Elementar, Germany). The correlation of MC-LR molecular properties and its potential transformation pathway was computed by ChemBioDraw Ultra version 2015 (Tang et al. 2016). The detailed calculation procedure is presented in Text S3.

Toxicity assay

The biological toxicity of MC-LR and its degrading intermediate mixture was evaluated using colorimetric protein phosphatase inhibition assay (Heresztyn and Nicholson 2001). The samples for analysis included (1) $100 \mu\text{g L}^{-1}$ MC-LR solution, and (2) corresponding degrading intermediate mixtures after different times UV/ H_2O_2 treatment. The preparation and assay procedure of protein phosphatase 1 (PP1) and protein phosphatase 2A (PP2A) followed the same processes described in Zong et al. (2013). The assay was performed by adding $100 \mu\text{L}$ solution (prepared by dilution of the stock solutions) to $10 \mu\text{L}$ PP1/PP2A solution in a 96-well polystyrene micro-well plate.

Results and discussion

Control and degradation experiments of MC-LR

The results of three control experiments are presented in Fig. S2. Only slight variations of MC-LR concentration were observed. Notably, no significant degradation of MC-LR was observed after 265 nm UV-LED treatment. The results of UV-LED/ H_2O_2 degradation experiments are presented in Fig. 2a. The removal efficiencies all reached $\sim 99\%$ within 60 min. For $100 \mu\text{g L}^{-1}$ MC-LR, the removal efficiency reached approximately 99% ($<1 \mu\text{g L}^{-1}$) at 20 min. As shown in Table S3, the apparent rate constant of MC-LR degradation was in the range of 0.0663 to 0.2077 min^{-1} . The half-time was in the range of 3.3 to 10.5 min, suggesting that MC-LR can undergo fast

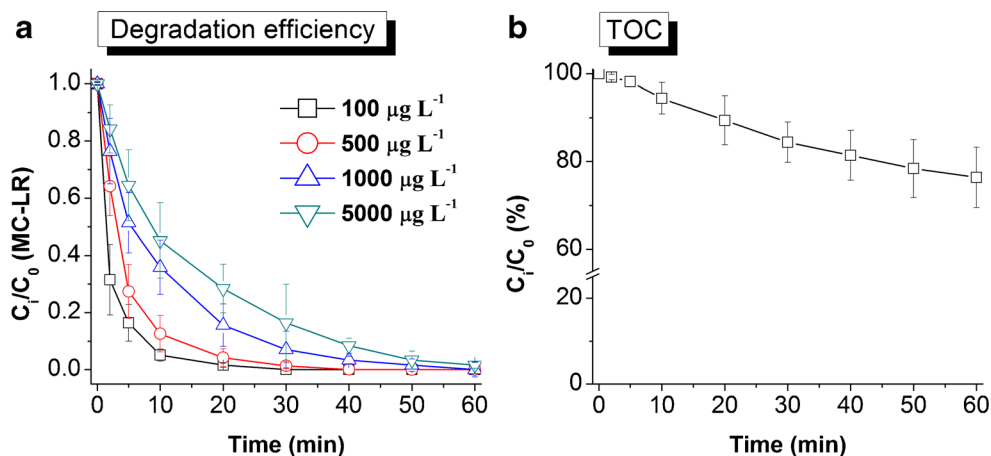


Fig. 2 Removal efficiency of MC-LR. **a** Different initial concentrations; **b** TOC variation. Experimental conditions: UV irradiating intensity $180 \mu\text{W cm}^{-2}$, solution volume 20 mL, solution temperature $25 \pm 2 \text{ }^\circ\text{C}$, pH 6.8–7.2, $[\text{MC-LR}]_0 = 0.1\text{--}5.0 \mu\text{M}$, and $[\text{H}_2\text{O}_2]_0 = 100 \mu\text{M}$. For TOC

experiment, only $[\text{MC-LR}]_0 = 5.0 \mu\text{M}$ was used. All the experiments were carried out in triplicate with *error bars* representing the standard error of the mean

degradation, which may ascribe to the promotion of $\text{OH}\cdot$ oxidation. Because the guideline value for MC-LR in drinking water is $1 \mu\text{g L}^{-1}$ (Ibelings et al. 2014), these results indicated that UV-LED/ H_2O_2 treatment may be a valid removal method for MC-LR.

The variation of TOC is presented in Fig. 2b. For 5 mg L^{-1} ($5 \mu\text{M}$) MC-LR solution, the apparent TOC value was $2.84 \pm 0.36 \text{ mg L}^{-1}$ at time zero. After 60 min reaction, only 24% TOC was removed in the 265 nm UV-LED/ H_2O_2 system. The incomplete mineralization can be attributed to the lack of H_2O_2 . The $[\text{H}_2\text{O}_2]/[\text{MC-LR}]$ was 20:1, which was lower than the basic stoichiometric molar ratio for total degradation. The low mineralization ratio implied the formation of intermediates.

MS² analysis of MC-LR

The MS² spectra of MC-LR and its intermediates have been reported in other studies (Diehnelt et al. 2005). The most common protonation sites of MC-LR were the methoxy group of Adda amino acid and the guanidine group of arginine, and thus, $[\text{MC-LR} + 2\text{H}]^{2+}$ and $[\text{MC-LR} + \text{H}]^+$ can both exist. According to the apparent mass-to-charge ratio equation (Eq. 2), $[\text{MC-LR} + \text{H}]^+$ and $[\text{MC-LR} + 2\text{H}]^{2+}$ had m/z of approximately 995.6 and 498.3, respectively. In the current study, the molecular formulas of $[\text{MC-LR} + \text{H}]^+$ and $[\text{MC-LR} + 2\text{H}]^{2+}$ were input into MasterView to acquire the relevant extracted ion chromatograms (EICs). It was found that $[\text{MC-LR} + 2\text{H}]^{2+}$ was the dominating ion in the current experiment.

$$\frac{m}{z} = \frac{M + nH}{n} \quad (2)$$

where m is the apparent mass of targeted ionized molecule, z is the electric charge of targeted ionized molecule, m/z represents the apparent mass-to-charge ratio, M is the exact mass of targeted molecule, n is the number of electric charge, and H represents the exact mass of a proton.

Eighty-five distinct fragments were observed (Fig. 3). To avoid redundancy, the top 20 fragments in term of intensity were selected (Table S6). Eighteen compositions were directly assigned to these fragments. The homolytic and heterolytic fragmentations of MC-LR resulted in different characteristic fragments. The fragment with a $m/z = 135.0799$ (so-called ADDA-135) had the highest intensity and was assigned as $[\text{C}_9\text{H}_{11}\text{O}]^+$. This fragment included the terminal benzene ring structure of Adda, which was reported as one of the most characteristic fragments of MC-LR (Diehnelt et al. 2005; Yuan et al. 1999). The fragment $m/z = 861.4844$ was assigned as $[\text{C}_{40}\text{H}_{65}\text{N}_{10}\text{O}_{11}]^+$, which was complementary to ADDA-135. The high intensities of these two fragments implied that the homolytic cleavage at $\text{C}_9\text{--}\text{C}_8$ was the dominating fragmentation of $[\text{MC-LR} + 2\text{H}]^{2+}$ (Yuan et al. 1999).

Several fragments with intact amino acid structure were observed. The fragment $m/z = 213.0877$ was assigned as $[\text{Glu} + \text{Mdha} + \text{H}]^+$ ($[\text{C}_9\text{H}_{13}\text{N}_2\text{O}_4]^+$), while the $m/z = 155.0818$ was assigned as $[\text{Mdha} + \text{Ala} + \text{H}]^+$ ($[\text{C}_7\text{H}_{11}\text{N}_2\text{O}_2]^+$). Irregular dissociations in amino acids were also observed. The fragment $m/z = 487.3004$ was assigned as $[\text{Ala} + \text{Leu} + \text{MeAsp} + \text{Arg} + \text{NH}]^+$ ($[\text{C}_{20}\text{H}_{39}\text{N}_8\text{O}_6]^+$). These characteristic fragments can provide useful information for subsequent intermediate interpretation.

Structure elucidation of intermediates

Three novel intermediates were observed, and their molecular formulas were identified as $\text{C}_{48}\text{H}_{74}\text{N}_{10}\text{O}_{15}$ (product A),

Spectrum from 20141218-1.wiff (sample 1) - Omin+AA, Experiment 7, +TOF MS² (100 - 1200) from 6.124 min
Precursor: 498.3 Da, CE: 35.0 CE=35

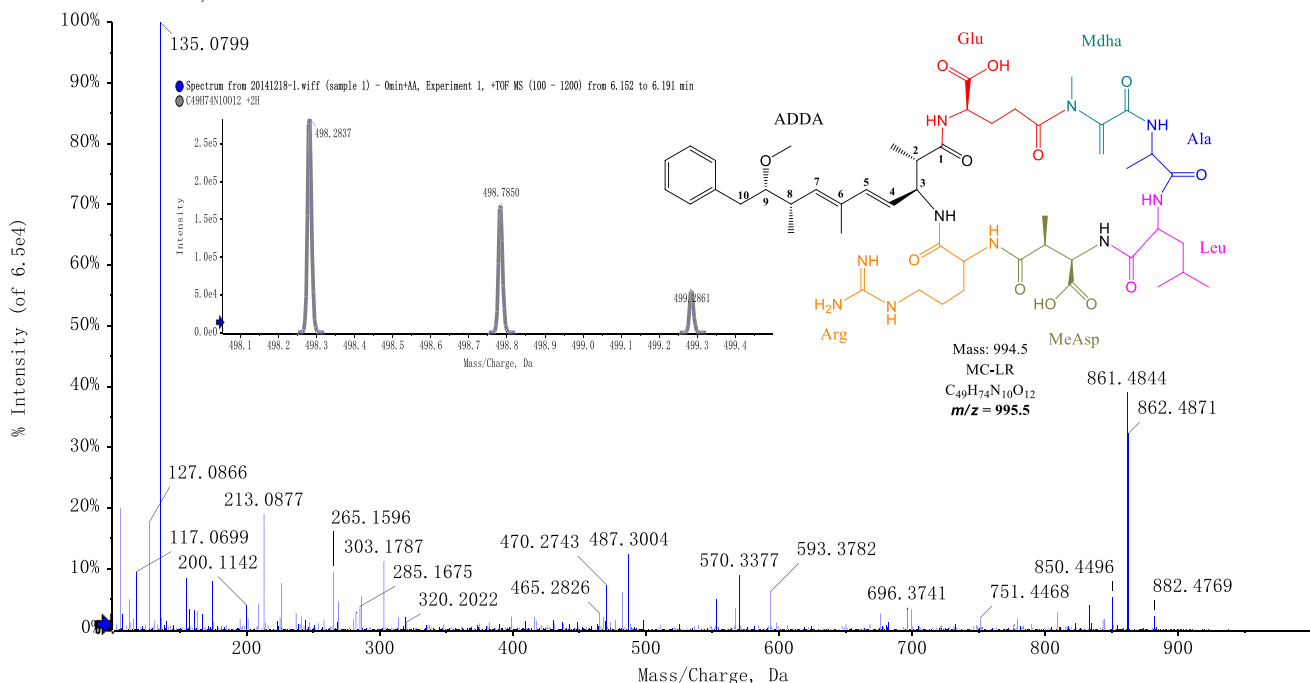


Fig. 3 MS² spectrum and isotope distribution of the $m/z = 498.2817$ ($[MC-LR + 2H]^{2+}/2$). In the isotope distribution graph, spectrum curve with *gray color* indicated the measured sample, and the spectrum curve with *blue color* indicated the extracted ion chromatography from the

measured sample, and the spectrum curve with *gray color* indicated the calculated ion chromatography of given molecular formula

$C_{36}H_{58}N_{10}O_{14}$ (product B), and $C_{33}H_{54}N_{10}O_{14}$ (product C) (Figs. 4, S4, and S5).

Product A has a $m/z = 516.2740$ for $[M + 2H]^{2+}/2$. This is the first report of this intermediate in UV-C/H₂O₂ or

Spectrum from 20141218-3.wiff (sample 1) - 5min+AA, Experiment 7, +TOF MS² (100 - 1200) from 5.100 min
Precursor: 516.3 Da, CE: 35.0 CE=35

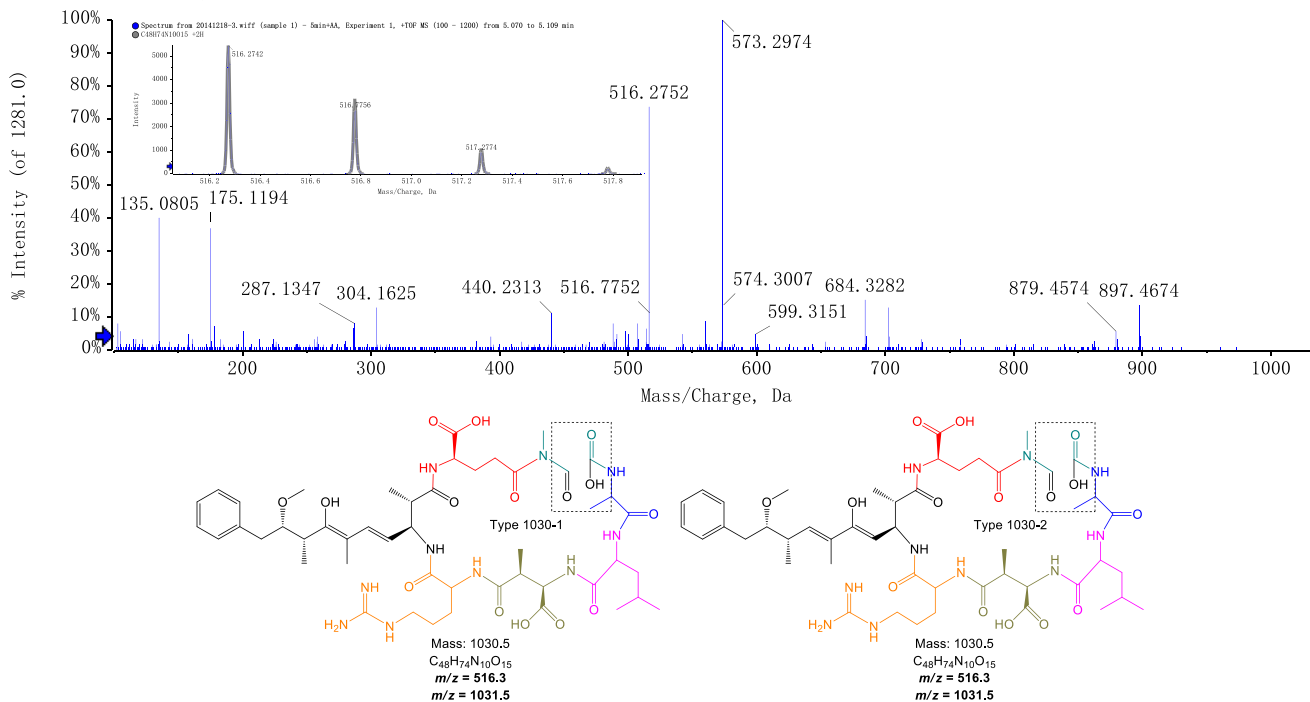


Fig. 4 Isotope distribution, MS² spectrum, and possible molecular structure of product A series (MW = 1030.5335 Da, RT = 5.100 min)

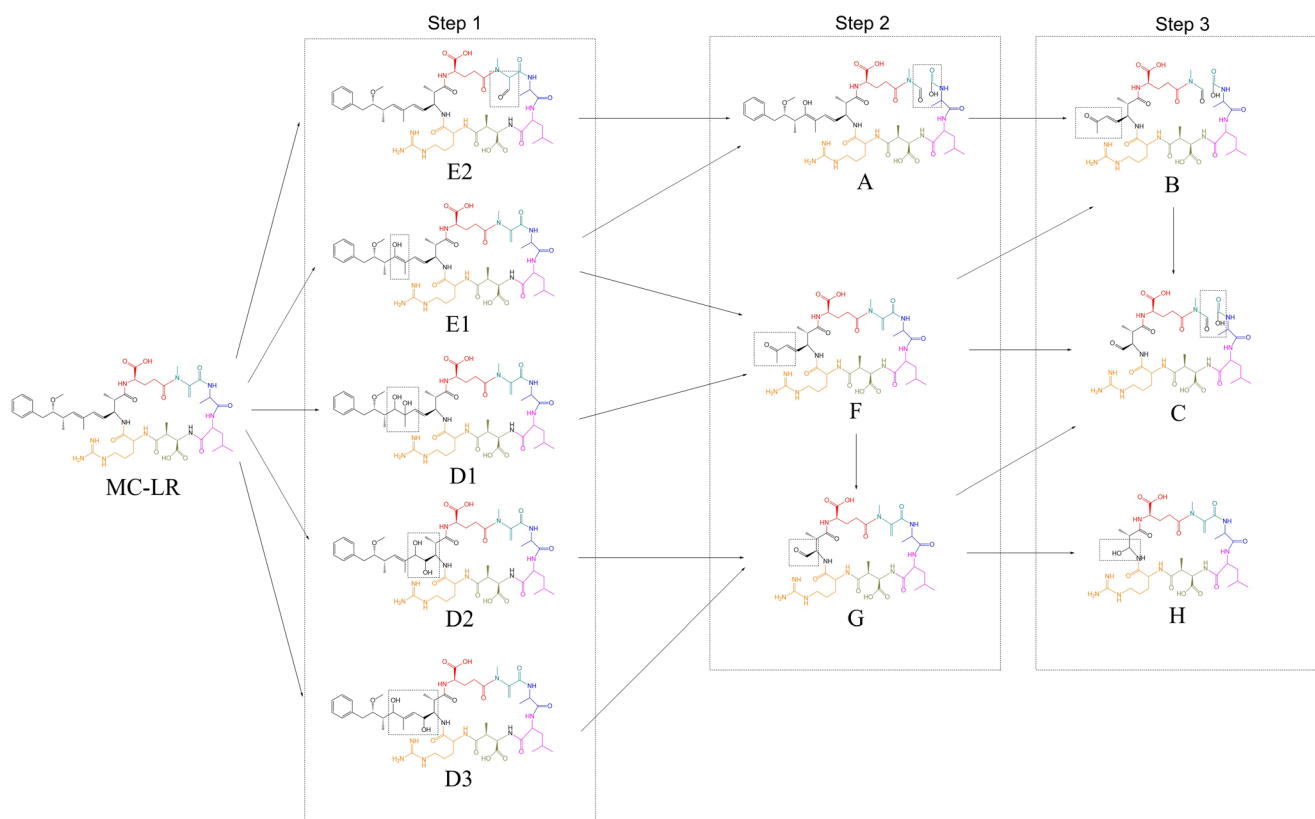
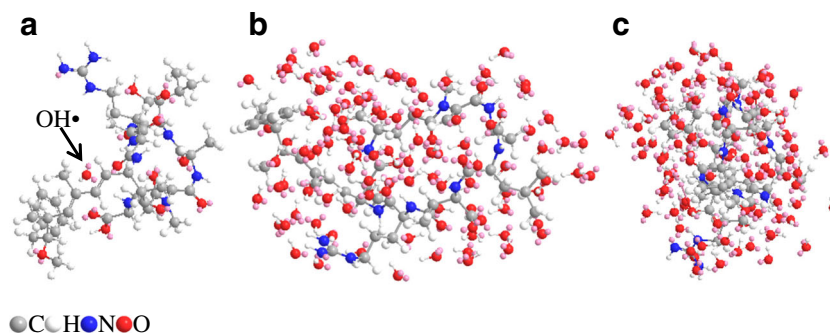


Fig. 5 Proposed generative pathways for the MC-LR intermediates

photocatalysis treatment of MC-LR. This intermediate had a molecular weight (MW) of 1030.5335, which differed by 35.9847 Da from MC-LR. According to the molecular formulas, the transformation from MC-LR to product A may involve an elimination of a carbon atom (-12 Da) and an addition of three oxygen atoms ($+48$ Da). The MS² fragments of product A included m/z 135.0805, 175.1194, 516.2752, 573.2974, 684.3282, 702.3385, 897.4636, etc. ADDA-135 represented the integrated Adda terminus, and its complementary fragment was m/z 897.4636, which also had a 35.9752 Da difference compared to its corresponding fragment (m/z 861.4884) in MC-LR. Therefore, the oxidized sites may be located at the C=C in Mdha and/or Adda side-chain.

C=C in Mdha was found to be susceptible under OH \cdot attack. The continuous oxidation of this site has been reported (Antoniou et al. 2008b), which included a sequential double hydroxylation of the Mdha, oxidation to aldehyde, and cleavage of the R₂C-COR bond, ultimately forming an intermediate with $m/z = 1015.5$ ($[M + H]^+$, C₄₈H₇₄N₁₀O₁₄, approximately 20 Da different from MC-LR; Fig. S3). This C₄₈H₇₄N₁₀O₁₄ was not observed in the current study; however, product A may have a similar Mdha residue. In this case, a 16-Da (an oxygen atom) difference still remained. The addition of this oxygen atom may be located at the C=C or phenyl of Adda side-chain. Based on these hypotheses, three possible oxidized candidates were proposed (Fig. S3). The two candidates, product A1 and product A2, which had the higher matching score

Fig. 6 Molecular interaction between MC-LR and OH \cdot . **a** One MC-LR molecule with one OH \cdot ; **b** one MC-LR molecule with 100 OH \cdot , observed from one direction; and **c** one MC-LR molecule with 100 OH \cdot , observed from another direction



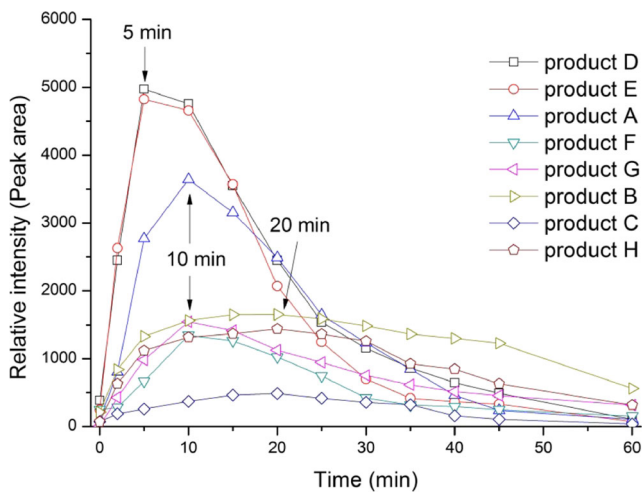


Fig. 7 Evolution curves for MC-LR and the observed intermediates. Experimental conditions: UV irradiating intensity $180 \mu\text{W cm}^{-2}$, solution volume 20 mL, solution temperature $25 \pm 2 \text{ }^\circ\text{C}$, pH 6.8–7.2, $[\text{MC-LR}]_0 = 5.0 \mu\text{M}$, and $[\text{H}_2\text{O}_2]_0 = 100 \mu\text{M}$

values (see in Supporting Information, both at 90.9%) were selected.

Product B ($m/z = 428.2140$ for $[\text{M} + 2\text{H}]^{2+}/2$) and product C ($m/z = 408.1983$ for $[\text{M} + 2\text{H}]^{2+}/2$) had single peaks at $\text{RT} = 4.648$ min and $\text{RT} = 4.280$ min, respectively. The MS^2 data showed that the primary fragments of product B included m/z 112.0857, 470.2763, 599.3156, etc., while the fragments of product C were m/z 130.0508, 301.1034, 515.2962, etc. By analyzing these fragments, it was deduced that these two intermediates may be the further oxidized products from product A. The Adda side-chain only retained a ketone structure ($-\text{C}_4\text{H}_5\text{O}$, product B) and an aldehyde structure ($-\text{CHO}$, product C).

Five published intermediates were also determined, and their molecular formulas were identified as $\text{C}_{49}\text{H}_{76}\text{N}_{10}\text{O}_{14}$ (product D), $\text{C}_{49}\text{H}_{74}\text{N}_{10}\text{O}_{13}$ (product E), $\text{C}_{37}\text{H}_{58}\text{N}_{10}\text{O}_{12}$ (product F), $\text{C}_{34}\text{H}_{54}\text{N}_{10}\text{O}_{12}$ (product G), and $\text{C}_{33}\text{H}_{54}\text{N}_{10}\text{O}_{12}$ (product H). Based on the HRMS data and the published literatures (Antoniou et al. 2008a; Antoniou et al. 2008b;

Fotiou et al. 2013; Liu et al. 2009; Yang et al. 2011), the possible structure of these products were identified (Figs. S6, S7, S8, S9, and S10).

Degradation pathway

A three-step degradation pathway of MC-LR by 265 nm UV-LED/ H_2O_2 was proposed (Fig. 5). In the first step, two series of intermediates were generated, including products E1, E2, D1, D2, and D3. The products D1, D2, and D3 were formed by the addition of two $\text{OH}\cdot$ and the loss of a $\text{C}=\text{C}$ bond on the Adda side-chain (Antoniou et al. 2008b; Merel et al. 2009). The molecular calculation results also confirmed that this $\text{C}=\text{C}$ bond was the primary target under the attack of $\text{OH}\cdot$ at the same molar concentration as MC-LR (Fig. 6a). When the molar ratio of $\text{OH}\cdot$ and MC-LR was 100 as the current study set, almost all the chemical bonds could be the potential targets (Fig. 6b, c). However, which bond would be broken is relied on the molecular structure of MC-LR. The products E1 and E2 had different generative mechanisms. Product E1 was formed by the hydroxyl substitution of the hydrogen at C_7 on the Adda side-chain. However, E2 may be a product that is formed by the attack of $\text{OH}\cdot$ on the $\text{C}=\text{C}$ of Mdha, resulting in the formation of an aldehyde structure (Antoniou et al. 2008b).

Three intermediates were observed during the second step, including product A series, product F, and product G. Product A series may be the additional oxidized products from product E1 and E2. Product E1 can be further oxidized at the $\text{C}=\text{C}$ of Mdha, while product E2 can be oxidized at the $\text{C}=\text{C}$ of Adda. The occurrence of product A series suggested that 265 nm UV-LED/ H_2O_2 can induce the synchronous oxidation on both sites of the Mdha and Adda side-chain. Product F may be a further oxidized intermediate of type product E2 or product D1, which was cut off at C_7 of the Adda side-chain and formed a ketone structure. Product G may be from product

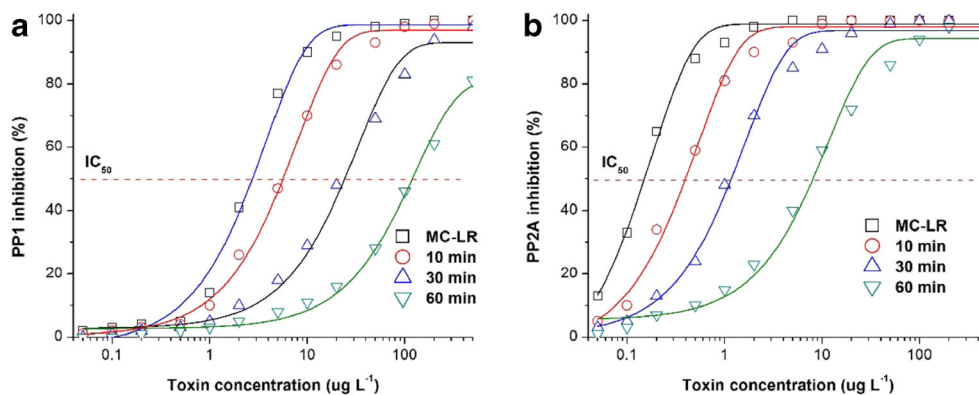


Fig. 8 Inhibition curves for MC-LR and degrading product mixtures. **a** PP1; **b** PP2A. Enzyme assays were conducted in triplicate, and the inhibition curves were plotted as percentage activity of PP1/PP2A based

on the control (without enzymes) versus MC-LR or degrading product mixture. IC_{50} values for MC-LR on PP1 and PP2A were 2.45 and $0.15 \mu\text{g L}^{-1}$, respectively

D2 or product D3, which was cut off at C₅ of Adda side-chain to form an aldehyde structure.

During the third step, three intermediates were observed, including products B, C, and H. The formation of product B was similar to product F with a breakage at C₇ of Adda side-chain, which may be the additional oxidized intermediate from product A series. Product C could be the additional oxidized intermediate from product F or product G, with a breakage at C₅ of the Adda side-chain and cleavage of the R₂C-COR of Mdha. Product H was formed by the total breakage of the Adda side-chain at C₃ from product G, resulting in the formation of a hydroxyl structure.

The conjugated C=C of Adda and the C=C of Mdha were the primary targets of the OH[•] attack in the 265 nm UV-LED/H₂O₂ treatment, forming the Adda residue and Mdha residue structures. MC-LR has been reported to irreversibly inhibit protein phosphatase 1 and protein phosphatase 2A in hepatic cells, resulting in the disruption of cell structure, intrahepatic hemorrhage, and death of mammals (Campos and Vasconcelos 2010, Gullidge et al. 2002). However, this toxicity relied on the intact structure of MC-LR. Among the seven amino acids, Adda played an important role in the biological activity of MC-LR due to its stereochemistry and hydrophobicity (Harada et al. 1990). Furthermore, the cyclic structure also contributed to the toxicity of MC-LR. Therefore, the breakages of the Adda side-chain and Mdha implied that the 265 nm UV-LED/H₂O₂ method was a valid degradation method for MC-LR.

Relative intensity variation of observed intermediates

Figure 7 presents the relative intensity variation tendency of the observed intermediates. The relative intensity of product D rapidly increased to $\sim 5.0 \times 10^3$ at 5 min and then decreased to lower than 5×10^2 within 60 min. Product E had a similar variation pattern. The relative intensity of product A increased in the initial 10 min and then slowly decreased. Products F and G also had highest intensities at approximate 10 min. For products B, C, and H, their relative intensities continuously increased in initial 30 min, followed by slight declines. These results suggested a generating sequence: (1) products D and E; (2) products A, F, and G; and (3) products B, C, and H. This sequence was in accordance with the proposed three-step consecutive oxidation pathway.

Biological toxicity evaluation of MC-LR and degrading intermediate mixture

The existences of degrading products may still have a potential risk to the environment due to their unknown toxicity. Due to the limited experimental condition, only the toxicological assessment of degrading intermediate mixture after different reaction times was performed using PP1 and PP2A as targets.

Based on the enzyme inhibition results, the inhibition curves were exponential fitted with the partial IC₅₀ indexes (Fig. 8). The IC₅₀ values for MC-LR on PP1 and PP2A were 2.45 and 0.15 $\mu\text{g L}^{-1}$, respectively, which were consistent with other researches (Zong et al. 2013). After UV/H₂O₂ reaction, the toxicity rank sequence was confirmed to follow the order: MC-LR > 10 min > 30 min > 60 min, both for PP1 and for PP2A. For PP1, the IC₅₀ values at 10, 30, and 60 min were 6.3, 22.3, and 103.5 $\mu\text{g L}^{-1}$, respectively. After 30 min reaction, the IC₅₀ was approximately 10 times higher than that of MC-LR. Similar result was observed in PP2A. These results indicated that the toxicity of degrading intermediate mixture was significantly lower than that of untreated MC-LR. Since the relative abundances of observed intermediates were still high at 30 min (Fig. 7), the incomplete degradation of MC-LR was seen to be effective for toxicity weakening.

EE/O calculation of UV-LED/H₂O₂ systems

The results of UV-LED/H₂O₂ treatment in terms of removal efficiency above were seen to be rather good (Fig. 2). However, it is necessary to evaluate its cost. The electrical energy per order (EE/O) values were calculated for 265 nm UV-LED/H₂O₂ system. Detailed information about the calculation method can be found in He et al. (2013) The EE/O value was calculated by taking into account of both electrical energy and chemical oxidant input into devices (Tan et al. 2014). The calculation results are shown in Table S7. The EE/O values were calculated to be in the range of 0.00447 to 0.00612 kWh m⁻³ order⁻¹ for 100–5000 $\mu\text{g L}^{-1}$ MC-LR degraded by 265 nm UV-LED/H₂O₂. These EE/O values were lower than the values in the degradation experiments of other organic contaminants using conventional mercury lamps (Tan et al. 2013; Tan et al. 2014).

Conclusion

To conclude, UV-LED/H₂O₂ was able to efficiently degrade MC-LR under different concentrations in the range of 100–5000 $\mu\text{g L}^{-1}$. Based on the high-resolution qTOF MS/MS data, a three-step screening was used to determine the intermediates. Three novel intermediates were found, and their structures were elucidated. The toxicity of MC-LR was weakened with a relative low mineralization, suggesting that 265 nm UV-LED/H₂O₂ was a useful method for MC-LR degradation.

Acknowledgments This project was supported by the Science and Technology Planning Project of Guangdong Province, China (Grant No. 2014A020216014) and the National Natural Science Foundation of China (Grant Nos. 51308224, 21577049).

References

- Antoniou MG, Shoemaker JA, Armah A, Dionysiou DD (2008a) LC/MS/MS structure elucidation of reaction intermediates formed during the TiO₂ photocatalysis of microcystin-LR. *Toxicol* 51:1103–1118
- Antoniou MG, Shoemaker JA, Cruz AA, Dionysiou DD (2008b) Unveiling new degradation intermediates/pathways from the photocatalytic degradation of microcystin-LR. *Environ Sci Technol* 42:8877–8883
- Campos A, Vasconcelos V (2010) Molecular mechanisms of microcystin toxicity in animal cells. *Int J Mol Sci* 11:268–287
- Chang J, Z-l C, Wang Z, Shen J-m, Chen Q, Kang J, Yang L, X-w L, C-x N (2014) Ozonation degradation of microcystin-LR in aqueous solution: intermediates, byproducts and pathways. *Water Res* 63:52–61
- Chiou CS, Chang CT, Chang CC, Chang CY (2008) Photodegradation kinetics of formaldehyde using light sources of UVA, UVC and UVLED in the presence of composed silver titanium oxide photocatalyst. *J Hazard Mater* 155:164–172
- Christoffersen K, Kaas H (2000) Toxic cyanobacteria in water. A guide to their public health consequences, monitoring, and management. *Limnol Oceanogr* 87(5):255–258
- de Freitas AM, Sirtori C, Lenz CA, Zamora PGP (2013) Microcystin-LR degradation by solar photo-Fenton, UV-A/photo-Fenton and UV-C/H₂O₂: a comparative study. *Photochemical & Photobiological Sciences* 12:696–702
- Diehnelt CW, Peterman SM, Budde WL (2005) Liquid chromatography–tandem mass spectrometry and accurate *m/z* measurements of cyclic peptide cyanobacteria toxins. *Trac-trend Anal Chem* 24:622–634
- Fotiou T, Triantis TM, Kaloudis T, Pastrana-Martinez LM, Likodimos V, Falaras P, Silva AM, Hiskia A (2013) Photocatalytic degradation of microcystin-LR and off-odor compounds in water under UV-A and solar light with a nanostructured photocatalyst based on reduced graphene oxide–TiO₂ composite. Identification of intermediate products. *Ind Eng Chem Res* 52:13991–14000
- Gulledge B, Aggen J, Huang H, Nairn A, Chamberlin A (2002) The microcystins and nodularins: cyclic polypeptide inhibitors of PPI and PP2A. *Curr Med Chem* 9:1991–2003
- Harada K, Ogawa K, Matsuura K, Murata H, Suzuki M, Watanabe MF, Itezono Y, Nakayama N (1990) Structural determination of geometrical isomers of microcystins LR and RR from cyanobacteria by two-dimensional NMR spectroscopic techniques. *Chem Res Toxicol* 3:473–481
- He XX, de la Cruz AA, Dionysiou DD (2013) Destruction of cyanobacterial toxin cylindrospermopsin by hydroxyl radicals and sulfate radicals using UV-254 nm activation of hydrogen peroxide, persulfate and peroxymonosulfate. *Journal of Photochemistry and Photobiology A—Chemistry* 251:160–166
- Heresztyn T, Nicholson BC (2001) Determination of cyanobacterial hepatotoxins directly in water using a protein phosphatase inhibition assay. *Water Res* 35:3049–3056
- Ibelings BW, Backer LC, Kardinaal WEA, Chorus I (2014) Current approaches to cyanotoxin risk assessment and risk management around the globe. *Harmful Algae* 40:63–74
- Izadifard M, Achari G, Langford CH (2013) Application of photocatalysts and LED light sources in drinking water treatment. *Catalysts* 3:726–743
- Jamali A, Vanraes R, Hanselaer P, Gerven TV (2013) A batch LED reactor for the photocatalytic degradation of phenol. *Chemical Engineering & Processing Process Intensification* 71:43–50
- Jo WK, Tayade RJ (2014) New generation energy-efficient light source for photocatalysis: LEDs for environmental applications. *Ind Eng Chem Res* 53:2073–2084
- Kaya K, Sano T (1998) A photodetoxification mechanism of the cyanobacterial hepatotoxin microcystin-LR by ultraviolet irradiation. *Chem Res Toxicol* 11:159–163
- Liu I, Lawton LA, Bahnmann DW, Liu L, Proft B, Robertson PK (2009) The photocatalytic decomposition of microcystin-LR using selected titanium dioxide materials. *Chemosphere* 76:549–553
- Merel S, LeBot B, Clément M, Seux R, Thomas O (2009) MS identification of microcystin-LR chlorination by-products. *Chemosphere* 74:832–839
- Repo E, Rengaraj S, Pulkka S, Castangnoli E, Suihkonen S, Sopanen M, Sillanpää M (2013) Photocatalytic degradation of dyes by CdS microspheres under near UV and blue LED radiation. *Separation & Purification Technology* 120:206–214
- Tan C, Gao N, Yang D, Zhang Y, Sui M, Jing D, Zhou S (2013) Degradation of antipyrine by UV, UV/H₂O₂ and UV/PS. *J Hazard Mater* 260:1008–1016
- Tan CQ, Gao NY, Zhou SQ, Xiao YL, Zhuang ZZ (2014) Kinetic study of acetaminophen degradation by UV-based advanced oxidation processes. *Chem Eng J* 253:229–236
- Tang L, Wang L, Ou H, Li Q, Ye J, Yin H (2016) Correlation among phenyltins molecular properties, degradation and cellular influences on *Bacillus thuringiensis* in the presence of biosurfactant. *Biochem Eng J* 105:71–79
- Tayade RJ, Natarajan TS, Bajaj HC (2009) Photocatalytic degradation of methylene blue dye using ultraviolet light emitting diodes. *Ind Eng Chem Res* 48:10262–10267
- Tsuji K, Watanuki T, Kondo F, Watanabe MF, Suzuki S, Nakazawa H, Suzuki M, Uchida H, Harada K-I (1995) Stability of microcystins from cyanobacteria-II. Effect of UV light on decomposition and isomerization. *Toxicol* 33:1619–1631
- USEPA (2007) Toxicological reviews of cyanobacterial toxins: anatoxin-A, cylindrospermopsin and microcystins (LR, RR, YR and LA). Office of Water, USEPA, Washington
- Vilhunen S, Sillanpää M (2010) Recent developments in photochemical and chemical AOPs in water treatment: a mini-review. *Rev Environ Sci Bio* 9:323–330
- Vilhunen SH, Sillanpää ME (2009) Ultraviolet light emitting diodes and hydrogen peroxide in the photodegradation of aqueous phenol. *J Hazard Mater* 161:1530–1534
- Yang J, Chen D, Deng A, Huang Y, Chen C (2011) Visible-light-driven photocatalytic degradation of microcystin-LR by Bi-doped TiO₂. *Res Chem Intermediat* 37:47–60
- Yuan M, Namikoshi M, Otsuki A, Rinehart KL, Sivonen K, Watanabe MF (1999) Low-energy collisionally activated decomposition and structural characterization of cyclic heptapeptide microcystins by electrospray ionization mass spectrometry. *J Mass Spectrom* 34:33–43
- Zhou S, Shao Y, Gao N, Li L, Deng J, Zhu M, Zhu S (2014) Effect of chlorine dioxide on cyanobacterial cell integrity, toxin degradation and disinfection by-product formation. *Sci Total Environ* 482:208–213
- Zong W, Sun F, Sun X (2013) Oxidation by-products formation of microcystin-LR exposed to UV/H₂O₂: toward the generative mechanism and biological toxicity. *Water Res* 47:3211–3219